Applied Physics Letters

Multiple coherent dispersive waves generation in silicon nitride slot waveguide

Cite as: Appl. Phys. Lett. **120**, 071103 (2022); https://doi.org/10.1063/5.0073683
Submitted: 02 October 2021 • Accepted: 03 February 2022 • Published Online: 15 February 2022

Yuxi Fang, Changjing Bao, Zhi Wang, et al.

Applied Physics Letters ARTICLE scitation.org/journal/apl

Multiple coherent dispersive waves generation in silicon nitride slot waveguide

Cite as: Appl. Phys. Lett. **120**, 071103 (2022); doi: 10.1063/5.0073683
Submitted: 2 October 2021 · Accepted: 3 February 2022 ·
Published Online: 15 February 2022

Yuxi Fang,[1] Changjing Bao,[2] Zhi Wang,[1] Weigang Zhang,[1] Zhongqi Pan,[3] and Yang Yue[4,a)]

AFFILIATIONS

[1]Institute of Modern Optics, Nankai University, Tianjin 300350, China
[2]Department of Electrical Engineering, University of Southern California, Los Angeles, California 90089, USA
[3]Department of Electrical & Computer Engineering, University of Louisiana at Lafayette, Lafayette, Louisiana 70504, USA
[4]School of Information and Communications Engineering, Xi'an Jiaotong University, Xi'an 710049, China

[a)]Author to whom correspondence should be addressed: yueyang@xjtu.edu.cn

ABSTRACT

A method to generate multiple dispersive waves (DWs) with pumping in a normal dispersion regime is proposed. We show flexibility of producing four DWs in a silicon nitride (Si_3N_4) slot waveguide and explain the underlying dynamics of a four DWs generation process in detail, i.e., DWs emission via the optical wave-breaking phenomenon in an anomalous dispersion regime. Compression of the first anomalous DW results in the subsequent cascade DW generation. Combined with the soliton induced blue-shifted dispersive wave and red-shifted dispersive wave, the spectrum spans from visible to mid-IR with high coherence. The four DWs generation process has agreement with prediction of the phase-matching condition. Overall, this multiple DWs generation method in a Si_3N_4 waveguide provides the possibility for having an efficient, compact, and coherent mid-IR light source.

Compared with fiber-based platforms, integrated photonics offer key advantages for enabling nonlinear processes, which include high effective nonlinearities, low power consumption, compact size, and potential possibilities for large-scale implementation of integrated devices.[1–4] Among the plentiful integrated nonlinear platforms, a silicon nitride (Si_3N_4) waveguide is a promising one due to its material compatibility with existing complementary metal-oxide-semiconductor (CMOS) fabrication technology.[5–7] In addition, Si_3N_4 is free from two-photon absorption in the near-infrared regime,[8,9] and the generated spectrum allows one to be extended to mid-infrared (mid-IR) wavelengths;[10] thus, it is suitable for broadband nonlinear applications.

Dispersive wave (DW) generation is a phase-matching process perturbed by higher-order dispersion.[11–14] DW generation is an effective mechanism to obtain additional spectrum components with high coherence.[15–18] Conventionally, DW emission is described as when a higher-order soliton breaks into its fundamental solitons, and then the energy transfers from the soliton to narrow-band resonance in the normal dispersion region.[19,20] Pumping in the anomalous dispersion is a primary condition to form solitons.[21–25] Additionally, the generation of DWs is possible when pumping in the normal group velocity dispersion (GVD) regime.[26–32] The directional spectrum could pass through the anomalous dispersion regime and then generate the DWs in the other normal dispersion regime in Refs. 30–32. DW emission in the anomalous dispersion regime was shown to occur with dark soliton propagating.[29] The non-solitonic pulse can also produce a narrow-band DW in the anomalous dispersion region[33–38] when pumping in the normal dispersion region. In this case, optical wave-breaking (OWB) is the key mechanism.[33–35]

In this paper, we investigate the four DWs radiation phenomenon and explain the underlying mechanism in detail when pumping in the normal dispersion regime based on a Si_3N_4 horizontal slot waveguide. Four DWs are generated spanning from visible (600 nm) to mid-IR (4500 nm), via multiple DWs radiation in both anomalous and normal dispersion regions. The position of the DWs could be tailored over a broad wavelength by phase-matching condition engineering, and the spectra are shown to have a high degree of coherence. This four DWs generation method in the Si_3N_4 waveguide provides the potential possibility of obtaining more DWs by tailoring the dispersion and explains the mechanism of multiple DWs generation based on the interaction between weak dispersion and Kerr nonlinearity.

Figure 1 shows the schematic of the multiple DWs generation process in the proposed Si_3N_4 slot waveguide. When a short pulse with kilowatt peak power propagates through the designed Si_3N_4 slot waveguides, the four DWs generation process can be implemented within a few millimeters distance. The chromatic dispersion (CD) curve of multiple DWs generation is also indicated. The saddle-shaped CD profile with higher peaks on the left shoulder forms a narrow low anomalous dispersion. We pump the input pulse in the normal GVD regime. Two DWs are emitted in the normal dispersion regime, and two DWs are formed in the anomalous dispersion regime. Figure 1 depicts the cross section of the proposed Si_3N_4 horizontal slot waveguide structure. The material refractive indices of Si, SiO_2, and Si_3N_4 are obtained by using the Sellmeier equations.[39,40] The refractive index of Si_3N_4 is close to that in the low pressure chemical vapor deposition (LPCVD) Si_3N_4 films.[41] Compared with the strip waveguide, a slot waveguide provides more design freedom to tailor the CD, which is beneficial for plentiful nonlinear phenomena. W, H, H_u, H_s, and H_l represent the waveguide width, waveguide height, upper Si_3N_4 thickness, middle SiO_2 slot thickness, and lower Si_3N_4 thickness, respectively.

Importantly, the phase-matching condition determines the position and the number of DWs. The phase-matching argument requires the DW propagating with the same phase velocity as that of the soliton. If ω and ω_s are the frequencies of the DWs and solitons, the equation is usually expressed as[42]

$$\beta(\omega) = \beta(\omega_s) + \beta_1(\omega - \omega_s) + \frac{1}{2}\gamma P_s, \tag{1}$$

where $\beta(\omega)$ is the propagation constant in the waveguide, γ is the Kerr nonlinear coefficient, and P_s is the peak power of the soliton pulse. The last constant term ($\frac{1}{2}\gamma P_s$) in Eq. (1) can be defined as C. Equation (1) can also be rewritten to express the phase mismatch between the DW and the soliton as

$$\Delta\beta(\omega) = \beta(\omega) - \beta(\omega_s) - \beta_1(\omega - \omega_s) - C$$
$$= \sum_{n=2} \frac{(\omega - \omega_s)^n}{n!} \frac{d^n}{d\omega^n} \beta(\omega_s) - C. \tag{2}$$

We define the constant as C_0 when the peak power of the fundamental soliton is ignored. In this case, we can obtain the extremum of the phase-matching condition and predict the possibilities of multiple DWs generation by adjusting suitable peak power. The frequency changes of DWs due to intrapulse Raman scattering can be negligible in the Si_3N_4 waveguide. A high order polynomial provides the possibility to have multiple real solutions. We design the geometric parameters of the Si_3N_4 slot waveguide and, thus, tailor the overall dispersion and phase-matching condition of the waveguide for tuning the number and position of DWs.

First, we engineer the dispersion curve for phase matching in the nonlinear processes based on the flexibility of the proposed waveguide. Figure 2(a) shows the CD of the fundamental TM mode in a Si_3N_4 slot waveguide with 980 × 1800 cross sections. The optimized waveguide parameters are $W = 980$ nm, $H_u = 600$ nm, $H_s = 160$ nm, and $H_l = 1040$ nm. The higher peak of the saddle-shaped dispersion profile on the left shoulder is 50.96 ps/(nm·km) at 1240 nm. A narrow anomalous dispersion regime is formed between two zero-dispersion wavelengths (ZDWs) at 1035 and 1649 nm. A 880-nm pump pulse is launched in the normal dispersion regime. Furthermore, we calculate the nonlinear coefficient γ vs wavelength using a full-vector model[43] and use the measurement data of nonlinear refractive indices n_2 for Si_3N_4 and SiO_2 in Refs. 9 and 44. The nonlinear coefficient γ decreases

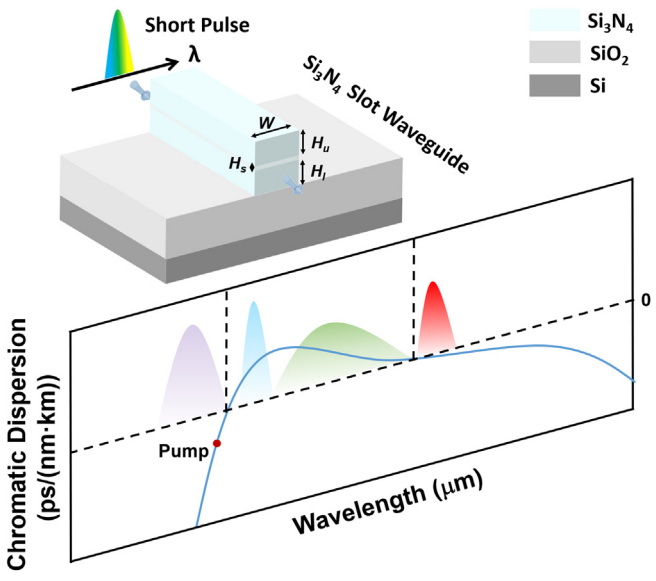

FIG. 1. Schematic of the four DWs generation process in the proposed Si_3N_4 slot waveguide.

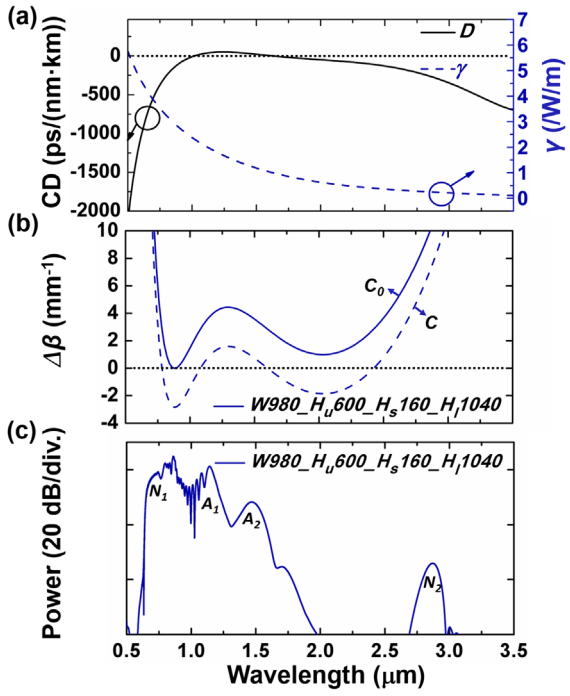

FIG. 2. (a) CD and nonlinear coefficient γ, (b) phase mismatch $\Delta\beta(\omega)$, and (c) simulated spectrum including four DWs in the proposed waveguide with the parameters of $W = 980$ nm, $H_u = 600$ nm, $H_s = 160$ nm, and $H_l = 1040$ nm.

with the wavelength due to the increase in the effective mode field area, which increases from 0.52 to 3.41 μm^2 as the wavelength increases from 500 to 3500 nm. At 880 nm, the effective mode area is 0.61 μm^2, and the corresponding nonlinear coefficient γ is 2.85/W/m.

We further calculate the profiles of phase mismatch $\Delta\beta(\omega)$ of Eq. (2) in Fig. 2(b). The solid line represents that the constant is C_0, i.e., the peak power of solitons is negligible in simulation. When the solutions of the phase-matching condition are sensitive to the soliton peak power, it is necessary to consider constant C. However, the peak power of the soliton pulse is not easy to evaluate due to pulse distortion. We can observe the trend of $\Delta\beta(\omega)$ and the number of solutions by adjusting the values of C, as shown in the dashed line of Fig. 2(b). The process of four DWs generation can be predicted through the phase-matching condition, and the peak power adjustment provides the potential possibilities to generate four DWs. In a certain range, four DWs can be generated. However, the prediction of the phase matching point is rough, because the pulse keeps changing constantly and the soliton is no longer in an ideal state. In order to verify the observed four DWs in the phase matching condition, we simulate the corresponding spectrum based on the nonlinear Schrödinger equation (NLSE). A chirp-free hyperbolic secant pulse centered at 880 nm with a FWHM of 100 fs and a peak power of 5 kW is launched into the above 1-cm long slot waveguide. The spectrum is broadened with generation of four obvious separated peaks near 700, 1140, 1470, and 2870 nm, respectively. The confinement loss at 2870 nm is 2.05 dB/cm. According to the position of DWs, we divide four DWs into two types, i.e., the DWs in normal and anomalous dispersion regions, marked as point N and A in Fig. 2(c), respectively. The positions of four DWs agree with the phase-matching point roughly.

In Fig. 3, we plot the temporal and spectral evolutions of the pulse as a function of the propagation length. One can obviously observe two DWs emitting at the normal dispersion region, and the locations are on the both sides of the pump in Fig. 3(b). In addition, we can clearly see that after approximately 1-cm propagation, a distinct component on the long-wavelength side is separated from the pump and transfers to the anomalous dispersion region, i.e., the first DW generation in anomalous dispersion (A_1). At 1470 nm, the temporal pulse compression of A_1 results in cascaded DW formation (A_2) with relatively low intensity, as illustrated in Fig. 3(a). Due to the strong temporal broadening of the normal dispersion, the intensity of cascaded DW A_2 has already been reduced.

To better visualize the process of four DWs generation, we simulate the XFROG pattern, which allows a convenient derivation of both temporal and frequency evolutions. In this case, the input pulse is pumped at the normal dispersion regime, which is close to the first zero-dispersion point (1035 nm). The spectrum is broadened by self-phase modulation (SPM) initially. As shown in Fig. 4(a), the SPM-induced chirp introduces spectral oscillations at the pulse's edges.[45] The following occurred dynamics can be divided into two parts. In the first part, under the action of normal GVD, the intermediate pulse sections propagate faster than the leading pulse tail, which results in the faster intermediate section overlap the slower preceding tail, forming the OWB phenomenon,[45] as seen in Fig. 4(b). Especially, pumping in the normal dispersion region can directly excite DWs in the anomalous dispersion regime, as described in Refs. 28, 33, and 36. We can observe the first DW in anomalous dispersion (A_1) emission from the OWB on the leading pulse edge in Fig. 4(b). The phase-matching rules

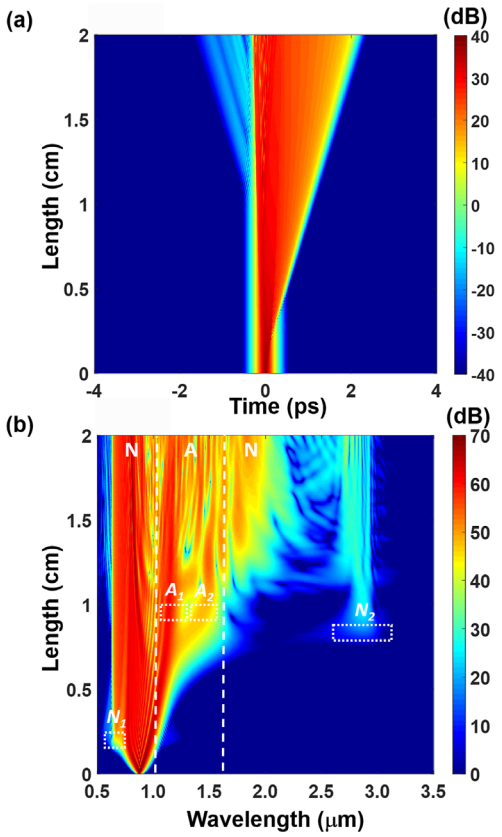

FIG. 3. (a) Temporal and (b) spectral evolutions along the waveguide with the parameters of $W = 980$ nm, $H_u = 600$ nm, $H_s = 160$ nm, and $H_l = 1040$ nm. The four DWs generation process including two anomalous DWs and two normal DWs generation.

between DWs and the dispersive shock waves (DSWs) could resonantly amplify the first anomalous DW A_1. In Fig. 3(a), one can also observe the oscillations of DSWs forming on the leading pulse edge, which is also shown in the time domain.[33] In Fig. 4(d), the energy flowing from A_1 to the cascaded DW A_2 can be seen, which results from temporal pulse compression.[46] In the second part, at some point, a part of energy in the normal dispersion region could flow into the anomalous dispersion region due to the SPM[30] and then forms solitons, as depicted in Fig. 4(c). Due to the perturbation from higher-order dispersion, the higher-order soliton breaks into fundamental components and accompanies with the DWs radiation in the normal dispersion regime. The energy transfers from the central wavelength of the soliton to the blue-shifted and red-shifted components. A blue-shifted dispersive wave (B-DW) and red-shifted dispersive wave (R-DW) can be clearly identified in Fig. 4(d).

The geometric parameters of the proposed slot waveguide are further modified to obtain the DW located at the longer wavelength. Larger waveguide relaxes the mode confinement, which leads to lower confinement loss in the long wavelength, enabling the DW in the further red wavelength. Under the larger and optimized geometric parameters ($W = 1200$ nm, $H_u = 810$ nm, $H_s = 195$ nm, and $H_l = 1195$ nm), the CD at the pump wavelength is −185.64 ps/(nm·km), and the

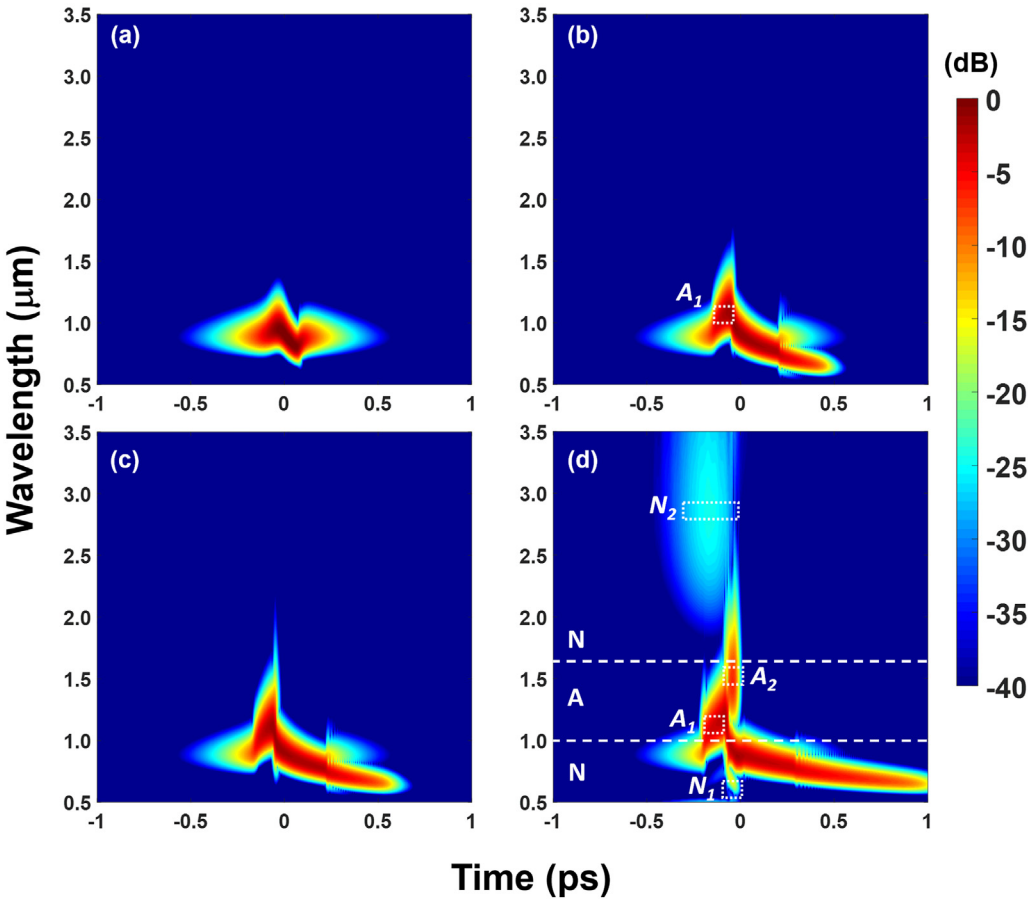

FIG. 4. Mixed spectral–temporal representation of the optical pulse at (a) 0.1, (b) 0.4, (c) 0.6, and (d) 1 cm.

nonlinear coefficient γ is 2.13/W/m at 880 nm in Fig. 5(a). Figure 5(b) also provides the prediction of four DWs generation. Three DWs are generated at long wavelengths, which align with the phase-matching points. In Fig. 5(c), it is obvious that the spectrum spans from the visible (650 nm) to the mid-IR (4200 nm) containing four DWs at both edges of the spectrum, and the locations of generated DWs are near 700, 1500, 2200, and 4200 μm. The input pulse is pumped at 880 nm with 5-kW peak power, and the waveguide length is 1.7 cm. Figure 6 shows the simulated spectral and temporal dynamics along the propagation when pumped in the normal dispersion region. The energy transfer process is similar, but the difference is the cascaded DW A_2 flowing to the normal dispersion regime, which is near to the second ZDW.

Next, in order to extend the furthest DW, we further engineer the dispersion and phase-matching point. The adjustable range of the phase-matching points for four DWs generation is wider in Fig. 7(a). We choose one of the representative geometers for tuning, i.e., waveguide upper Si_3N_4 thickness H_u modification to illustrate the influence of the geometric parameters on the phase-matching condition. When the upper Si_3N_4 thickness is increased, the change of the phase mismatch curve in the short wavelength region is small in its shape and position, while the curve moves up in the long wavelength range, and the phase-matching point continuously shifts toward shorter wavelengths. Figure 7(a) only depicts the phase-matching condition with C_0, and the prediction of four DWs generation is still reliable when considering constant term C, i.e., choosing suitable peak power. As illustrated in Fig. 7(b), we simulate the spectra of a 880-nm 100-fs input pulse in a 1.5-cm Si_3N_4 waveguide to observe the movement of the DWs along the phase-matching wavelength. The peak power of the input pulse is 10 kW, which increases significantly from the previous 5-kW pump pulse. Moreover, the intensity of DWs located at 4500 nm is relatively low, which is caused by the reduced frequency conversion efficiency between the center and the DW spectral components, and the higher confinement loss at longer wavelengths. Compared with confinement loss, the material loss of silica at the wavelength above 3500 nm is not the main reason.

Even though the intensity of the DWs is relatively low, we still observe the moving trend of the generated DWs as indicated by the phase-matching condition. The long-wave DW can cover up to 4500 nm. Further increasing the input pulse peak power is one of the effective ways to improve the power of the DWs. In Fig. 7(c), the overall spectral intensity of the generated DWs is greatly improved.

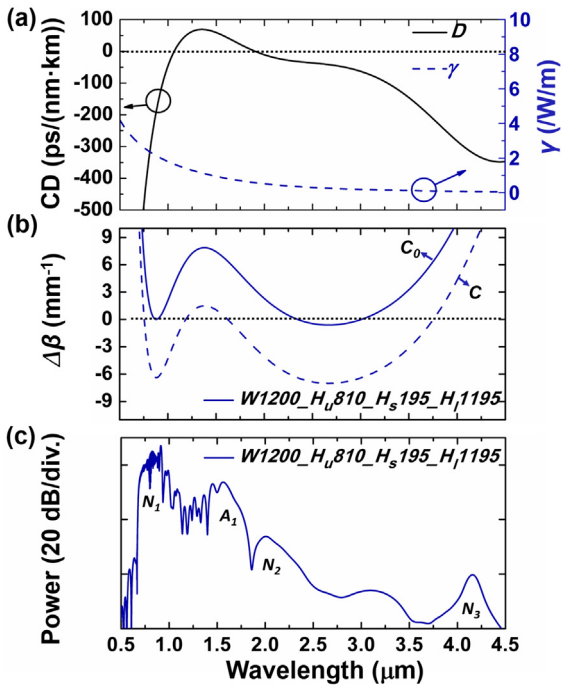

FIG. 5. (a) CD and nonlinear coefficient γ, (b) phase mismatch $\Delta\beta(\omega)$, and (c) simulated spectrum including four DWs in the proposed waveguide with the parameters of $W = 1200$ nm, $H_u = 810$ nm, $H_s = 195$ nm, and $H_l = 1195$ nm.

To assess the spectra coherence for the above three situations, we examine the coherence of the generated spectra using 40 simulations under identical conditions, except for the stochastic quantum noise of the input pulse.[47,48] The degree of coherence is calculated as[42]

$$g_{12}(\omega) = \frac{\langle \tilde{A}_1^*(L,\omega)\tilde{A}_2(L,\omega)\rangle}{\left[\langle|\tilde{A}_1(L,\omega)|^2\rangle\langle|\tilde{A}_2(L,\omega)|^2\rangle\right]^{1/2}}, \quad (3)$$

where $\tilde{A}_1$ and $\tilde{A}_2$ are the Fourier transforms of two neighboring pulses and the anglebrackets denote an average over the entire ensemble of pulses. As shown in Fig. 8, the position of the DWs could be tailored over a broad wavelength range with three optimized waveguide parameters, and the spectra maintain a high level of coherence over the entire bandwidth while pumping in the normal GVD regime. The coherence of OWB induced DWs and the subsequent cascaded DW are illustrated. The broadened spectrum in this regime has lower noise.[26] The highly coherent range is broader, as the long-wave DW is extended further. The extended spectral range as indicated above seems to be narrower than the wavelength range of the coherence, because the power is lower than the displayed vertical range. Nevertheless, the corresponding spectrum in the low power regime also demonstrates a high-level coherence. The inserted figure magnifies the edges of the coherence, which demonstrates random noise. The frequency components perform in an incoherent state when beyond the generated spectral region. In Fig. 8, we calculate the coherence of the spectra for a 100-fs input pulse, and we also illustrate the coherence can still maintain a high degree with increased pulse duration. In other words, the coherence of spectra, which broadens via

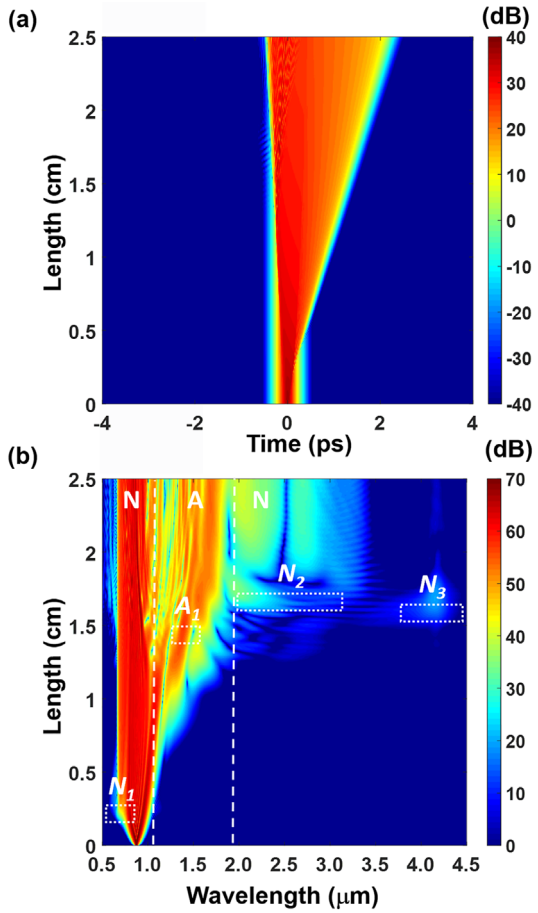

FIG. 6. (a) Temporal and (b) spectral evolutions along the waveguide with the parameters of $W = 1200$ nm, $H_u = 810$ nm, $H_s = 195$ nm, and $H_l = 1195$ nm. The four DWs generation process includes one anomalous DW and three normal DWs generation.

multiple DWs radiation, has the strong robustness for pulse widths and power.

In conclusion, we demonstrated the design freedom of the Si_3N_4 slot waveguide to control the number and position of DWs generation. By taking advantage of this flexibility, one could realize the nonlinear process of four DWs generation by pumping in the normal dispersion regime. These dynamics can be divided into two parts: First, OWB induces the first DWs emission in the anomalous dispersion regime and then the subsequent cascade DW generation via compression of the first anomalous DW. Second, the energy flows into the anomalous dispersion region induced B-DW and R-DW through soliton fission. The spectra can access the mid-IR region (4500 nm) through pumping at the visible wavelength. The high-level phase coherence of the spectrum for four DWs generation is verified numerically The results show the potential approaches to generate coherent spectra containing four DWs in the Si_3N_4 platform and also support the study of the correlation between the mechanism of four DWs generation and different CD curves. Si_3N_4 is further proved as a promising platform for integrated nonlinear photonics in the mid-IR. Our technique offers a possibility to form a high-power coherent source in the mid-IR range

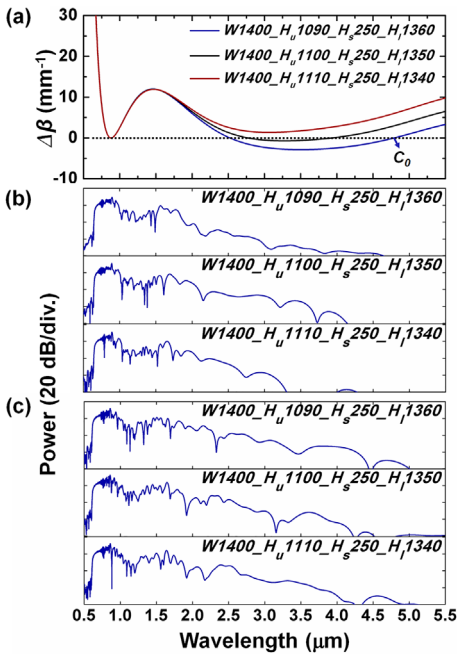

FIG. 7. (a) Phase mismatch $\Delta\beta(\omega)$ for waveguides with $W = 1400$ nm, $H_s = 250$ nm, and different H_u from 1090 to 1110 nm. Simulated spectrum with (b) 10-kW and (c) 15-kW input peak power.

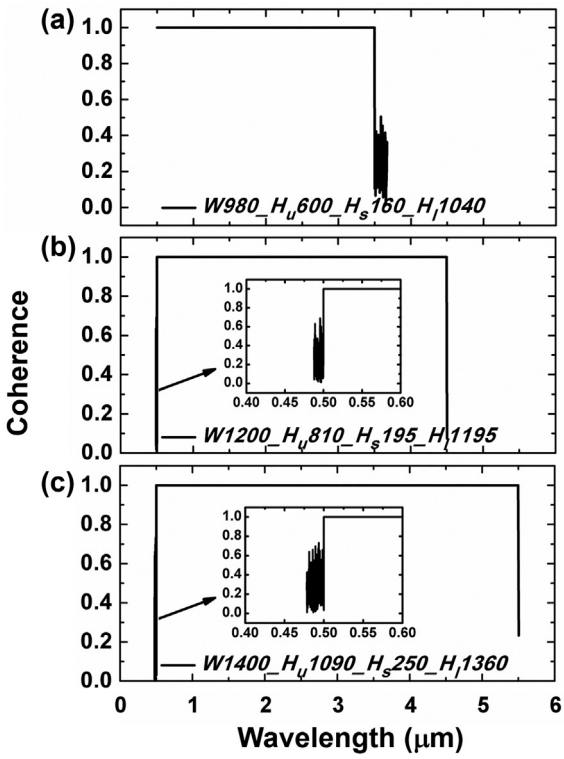

FIG. 8. Coherence of the generated spectra with four DWs generation. The furthest DW covers up to (a) 2870, (b) 4200, and (c) 4500 nm.

with various applications including precision metrology, spectroscopy, and optical frequency synthesis.

This work was supported in part by the National Key Research and Development Program of China (No. 2019YFB1803700); the Key Technologies R & D Program of Tianjin (No. 20YFZCGX00440); and the Fundamental Research Funds for the Central Universities, Nankai University (Nos. 63201178 and 63191511).

AUTHOR DECLARATIONS

Conflict of Interest

We have no conflicts of interest to disclose.

Author Contributions

Y.F. and C.B. contributed equally to this work.

DATA AVAILABILITY

The data that support the findings of this study are available from the corresponding author upon reasonable request.

REFERENCES

[1]M. Asghari and A. V. Krishnamoorthy, Nat. Photonics **5**, 268–270 (2011).
[2]C. Sun, M. T. Wade, Y. Lee, J. S. Orcutt, L. Alloatti, M. S. Georgas, A. S. Waterman, J. M. Shainline, R. R. Avizienis, and S. Lin, Nature **528**, 534–538 (2015).
[3]A. L. Gaeta, M. Lipson, and T. J. Kippenberg, Nat. Photonics **13**, 158–169 (2019).
[4]J. S. Levy, A. Gondarenko, M. A. Foster, A. C. Turner-Foster, A. L. Gaeta, and M. Lipson, Nat. Photonics **4**, 37–40 (2010).
[5]D. J. Moss, R. Morandotti, A. L. Gaeta, and M. Lipson, Nat. Photonics **7**, 597–607 (2013).
[6]H. Guo, C. Herkommer, A. Billat, D. Grassani, C. Zhang, M. H. Pfeiffer, W. Weng, C.-S. Bres, and T. J. Kippenberg, Nat. Photonics **12**, 330–335 (2018).
[7]D. Grassani, E. Tagkoudi, H. Guo, C. Herkommer, F. Yang, T. J. Kippenberg, and C.-S. Brès, Nat. Commun. **10**, 1553 (2019).
[8]D. Tan, K. Ikeda, P. Sun, and Y. Fainman, Appl. Phys. Lett. **96**, 061101 (2010).
[9]K. Ikeda, R. E. Saperstein, N. Alic, and Y. Fainman, Opt. Express **16**, 12987–12994 (2008).
[10]A. Z. Subramanian, E. Ryckeboer, A. Dhakal, F. Peyskens, A. Malik, B. Kuyken, H. Zhao, S. Pathak, A. Ruocco, and A. De Groote, Photonics Res. **3**, B47–B59 (2015).
[11]N. Akhmediev and M. Karlsson, Phys. Rev. A **51**, 2602 (1995).
[12]P. K. A. Wai, C. R. Menyuk, Y. Lee, and H. Chen, Opt. Lett. **11**, 464–466 (1986).
[13]P. K. A. Wai, C. Menyuk, H. Chen, and Y. Lee, Opt. Lett. **12**, 628–630 (1987).
[14]N. Singh, D. D. Hudson, and B. J. Eggleton, Opt. Express **23**, 17345–17354 (2015).
[15]A. R. Johnson, A. S. Mayer, A. Klenner, K. Luke, E. S. Lamb, M. R. Lamont, C. Joshi, Y. Okawachi, F. W. Wise, and M. Lipson, Opt. Lett. **40**, 5117–5120 (2015).
[16]F. Leo, S.-P. Gorza, S. Coen, B. Kuyken, and G. Roelkens, Opt. Lett. **40**, 123–126 (2015).
[17]P. Wang, J. Huang, S. Xie, J. Troles, and P. S. J. Russell, Photonics Res. **9**, 630–636 (2021).
[18]N. Singh, M. Xin, D. Vermeulen, K. Shtyrkova, N. Li, P. T. Callahan, E. S. Magden, A. Ruocco, N. Fahrenkopf, and C. Baiocco, Light Sci. Appl. **7**, 17131 (2018).
[19]I. Cristiani, R. Tediosi, L. Tartara, and V. Degiorgio, Opt. Express **12**, 124–135 (2004).
[20]A. Husakou and J. Herrmann, Phys. Rev. Lett. **87**, 203901 (2001).
[21]N. Singh, D. D. Hudson, Y. Yu, C. Grillet, S. D. Jackson, A. Casas-Bedoya, A. Read, P. Atanackovic, S. G. Duvall, and S. Palomba, Optica **2**, 797–802 (2015).

[22]Y. Zou, S. Chakravarty, C.-J. Chung, X. Xu, and R. T. Chen, Photonics Res. **6**, 254–276 (2018).
[23]R. Halir, Y. Okawachi, J. Levy, M. Foster, M. Lipson, and A. Gaeta, Opt. Lett. **37**, 1685–1687 (2012).
[24]L. Yin, Q. Lin, and G. P. Agrawal, Opt. Lett. **32**, 391–393 (2007).
[25]F. Leo, S.-P. Gorza, J. Safioui, P. Kockaert, S. Coen, U. Dave, B. Kuyken, and G. Roelkens, Opt. Lett. **39**, 3623–3626 (2014).
[26]G. Millot, S. Pitois, M. Yan, T. Hovhannisyan, A. Bendahmane, T. W. Hänsch, and N. Picqué, Nat. Photonics **10**, 27–30 (2016).
[27]Y. Okawachi, M. Yu, J. Cardenas, X. Ji, M. Lipson, and A. L. Gaeta, Opt. Lett. **42**, 4466–4469 (2017).
[28]K. Webb, Y. Xu, M. Erkintalo, and S. Murdoch, Opt. Lett. **38**, 151–153 (2013).
[29]T. Marest, C. M. Arabí, M. Conforti, A. Mussot, C. Milián, D. Skryabin, and A. Kudlinski, Opt. Lett. **41**, 2454–2457 (2016).
[30]S. Christensen, S. R. DS, O. Bang, and M. Bache, J. Opt. Soc. Am. B **36**, A131–A138 (2019).
[31]M. Meneghetti, C. R. Petersen, R. E. Hansen, A. I. Adamu, O. Bang, and C. Markos, Opt. Lett. **46**, 2533–2536 (2021).
[32]S. Bose, P. H. Reddy, J. Fan, A. Demircan, A. Ruehl, U. Morgner, S. Roy, M. Pal, S. K. Bhadra, and D. Ghosh, Appl. Opt. **59**, 9015–9022 (2020).
[33]M. Conforti and S. Trillo, Opt. Lett. **38**, 3815–3818 (2013).
[34]W. Tomlinson, R. H. Stolen, and A. M. Johnson, Opt. Lett. **10**, 457–459 (1985).
[35]D. Anderson, M. Desaix, M. Lisak, and M. L. Quiroga–Teixeiro, J. Opt. Soc. Am. B **9**, 1358–1361 (1992).
[36]M. Conforti, F. Baronio, and S. Trillo, Phys. Rev. A **89**, 013807 (2014).
[37]S. Malaguti, M. Conforti, and S. Trillo, Opt. Lett. **39**, 5626–5629 (2014).
[38]W. Wan, S. Jia, and J. W. Fleischer, Nat. Phys. **3**, 46–51 (2007).
[39]E. D. Palik, *Handbook of Optical Constants of Solids* (Academic Press, San Diego, 1998).
[40]T. Bååk, Appl. Opt. **21**, 1069–1072 (1982).
[41]L. Zhang, A. M. Agarwal, L. C. Kimerling, and J. Michel, Nanophotonics **3**, 247–268 (2014).
[42]G. P. Agrawal, *Nonlinear Fiber Optics* (Springer, New York, 2000).
[43]S. Afshar and T. M. Monro, Opt. Express **17**, 2298–2318 (2009).
[44]K. Kim, R. Stolen, W. Reed, and K. Quoi, Opt. Lett. **19**, 257–259 (1994).
[45]C. Finot, B. Kibler, L. Provost, and S. Wabnitz, J. Opt. Soc. Am. B **25**, 1938–1948 (2008).
[46]A. Bendahmane, F. Braud, M. Conforti, B. Barviau, A. Mussot, and A. Kudlinski, Optica **1**, 243–249 (2014).
[47]M. H. Frosz, Opt. Express **18**, 14778–14787 (2010).
[48]C. Huang, M. Liao, W. Bi, X. Li, L. Hu, L. Zhang, L. Wang, G. Qin, T. Xue, and D. Chen, Photonics Res **6**, 601–608 (2018).